Neural Network Modeling of Proton Exchange Membrane Fuel Cell

Sachin V. Puranik, *Member, IEEE*, Ali Keyhani, *Fellow, IEEE*, and Farshad Khorrami, *Senior Member, IEEE*

***Abstract*—This paper proposes a neural network model of a 500-W proton exchange membrane (PEM) fuel cell. The nonlinear autoregressive moving average model of the PEM fuel cell with external inputs is developed using the recurrent neural networks. The data required to train the neural network model is generated by simulating the nonlinear state space model of the 500-W PEM fuel cell. It is shown that the two-layer neural network, with a hyperbolic tangent sigmoid function, as an activation function, in the first layer, and a pure linear function, as an activation function, in the second layer can effectively model the nonlinear dynamics of the PEM fuel cell. After model is trained and validated, it is used to analyze the dynamic behavior of the PEM fuel cell. Finally, the effect of measurement noise on the performance of the neural network model is investigated, and the results are shown.**

***Index Terms*—Fuel cells, modeling, recurrent neural networks.**

NOMENCLATURE

a_0, a, b	Constants in Tafel equation (in volts per kelvin).
e	Number of participating electrons.
E^{Cell}	Reversible cell potential (in volts).
E_0^{Cell}	Standard reference potential at standard operating conditions (in volts).
F	Faraday's constant (in coulombs per mole).
I	Stack current (in amperes).
I_d	Current density (in amperes per square meter).
I_L	Limiting current (in amperes).
n_S	Number of PEM fuel cell stacks.
$P_{\mathrm{H_2}}$	Partial pressure of hydrogen (in atmosphere).
$P_{\mathrm{O_2}}$	Partial pressure of oxygen (in atmosphere).
$P_{\mathrm{H_2O}}$	Partial pressure of water (in atmosphere).
R	Universal gas constant (in joules per mole kelvin).
R^{Act}	Equivalent resistance corresponding to activation voltage loss (in ohms).
R^A	Resistance of anode (in ohms).
R^C	Resistance of cathode (in ohms).
R^{Conc}	Equivalent resistance corresponding to concentration voltage loss (in ohms).
R^O	Ohmic resistance (in ohms).
R_C^O	Constant in computation of R^O (in ohms).
R^M	Resistance of membrane (in ohms).
T	Stack temperature (in kelvins).
$u_{\mathrm{P_A}}$	Channel pressure of hydrogen (in atmosphere).
$u_{\mathrm{P_C}}$	Channel pressure of oxygen (in atmosphere).
$u_{\mathrm{T_R}}$	Room temperature (in kelvins).
V_C	Voltage across charge double-layer capacitor (in volts).
V_{fc}	Output voltage of PEM fuel cell (in volts).
$V_{O,\mathrm{FC}}$	Open-circuit output voltage (in volts).
$V_{\mathrm{loss}}^{\mathrm{Act}}$	Activation voltage loss (in volts).
V_{loss}^O	Ohmic voltage loss (in volts).
$V_{\mathrm{loss}}^{\mathrm{Conc}}$	Concentration voltage loss (in volts).
V_A^0	Voltage across anode (in volts).
V_C^0	Voltage across cathode (in volts).
V_M^0	Voltage across membrane (in volts).

Manuscript received February 19, 2008; revised February 07, 2009 and February 07, 2009; accepted September 28, 2009. Date of publication March 22, 2010; date of current version May 21, 2010. This work was supported in part by the National Science Foundation under Grant NSF ECS0501349. Paper no. TEC-00061-2008.

S. V. Puranik is with Hubbell Power Systems, Leeds, AL 35094 USA (e-mail: puranik.3@buckeyemail.osu.edu).

A. Keyhani is with the Department of Electrical and Computer Engineering, The Ohio State University, Columbus, OH 43210 USA (e-mail: keyhani.1@osu.edu).

F. Khorrami is with the Department of Electrical and Computer Engineering, Polytechnic University, Brooklyn, NY 11201 USA (e-mail: khorrami@smart.poly.edu).

Digital Object Identifier 10.1109/TEC.2009.2035691

I. INTRODUCTION

FUEL cell is an electrochemical energy conversion device that converts chemical energy into dc electrical energy. It is a clean energy source with low emissions, and low noise [1]. The first demonstration of a fuel cell was given by Sir William Grove in 1839, using electrolysis experiment and today, fuel cell is being looked upon as an environmental-friendly energy source, which can satisfactorily meet the growing energy needs of the 21st century [2]. Currently, fuel cells are being thoroughly researched worldwide, as they are considered to be the most promising candidates for developing distributed generation (DG) systems and hybrid vehicles. They can also be used in portable power and cogeneration applications [3]. Fuel cells are

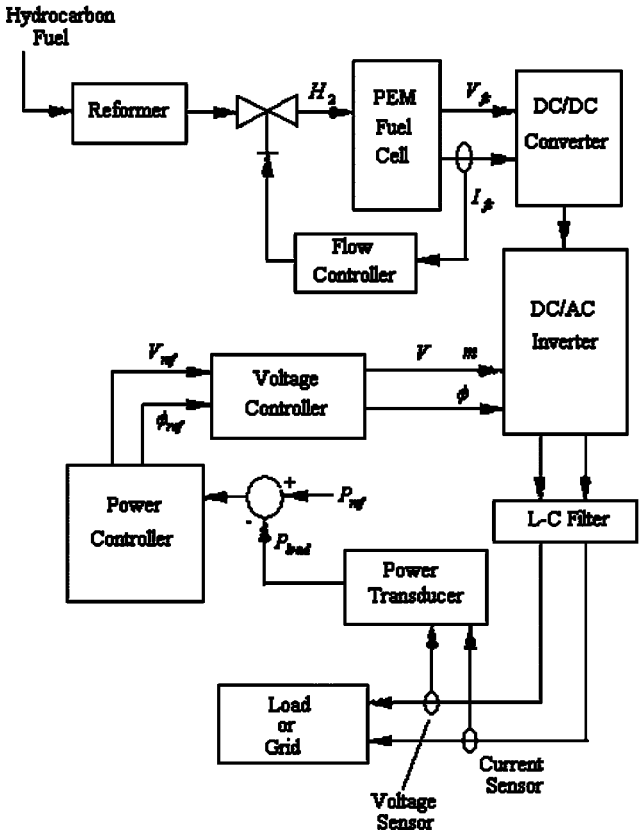

Fig. 1. PEM fuel cell-based DG system.

generally characterized by the type of electrolyte used by them. The different types of fuel cells available are—direct methanol fuel cells, alkaline fuel cells, proton exchange membrane (PEM) fuel cells, phosphoric acid fuel cells, molten carbonate fuel cells, solid oxide fuel cells, regenerative fuel cells, zinc air fuel cells, protonic ceramic fuel cells, and microbial fuel cells [2], [4]. Although all fuel cells are electrochemical energy conversion devices and operate on similar principle, each fuel cell type mentioned earlier has different operating characteristics, different materials of construction, different range of operating temperatures, and different applications.

Among the available fuel cells, PEM fuel cells offer excellent features, such as compact structure, high power density, solid electrolyte, low-operating temperature (50 ° C–100 °C), relatively fast start-up, low sensitivity to orientation, favorable power-to-weight ratio, long cell and stack life, and low corrosion [5]. Hence, PEM fuel cells have become an important choice for development of hybrid electric vehicles, fuel cell-based DG systems, and for various other emerging applications of fuel cells. The block diagram of the PEM fuel cell-based DG system is shown in Fig. 1 [6].

It is important to understand the dynamic behavior of the PEM fuel cell before it can be used in different applications. In the literature, some work is reported on modeling of the PEM fuel cell based on conventional modeling techniques. The work reported in [9]–[11] is focused on developing electrochemistry-based models of the PEM fuel cell. Analytical models of the PEM fuel cell are developed in [12]–[18]. However, compared to these conventional modeling techniques, a neural network approach provides certain unique modeling advantages. The electrochemistry-based PEM fuel cell models and analytical PEM fuel cell models make use of the first principles to model the dynamics of the PEM fuel cell, and the model development is based on modeling various electrochemical and thermodynamic processes inside the PEM fuel cell. The relationship between the PEM fuel cell's output voltage, stack temperature, and input variables is highly nonlinear. As a result, these PEM fuel cell models are generally complex and mathematically quite involved. Also, developing precise models using this approach requires proper knowledge of various process parameters, which are not always easily known. Moreover, it is fairly difficult to estimate these parameters for the PEM fuel cell system. The use of these models for PEM fuel cell system studies could be ineffective, unless right parameter values are known.

The neural network model, on the other hand, does not require knowledge of the process parameters. The neural network model can learn from a set of input–output data without the need of full specifications of the PEM fuel cell system. Once correctly trained, a neural network model can provide very good mapping between the output voltage, stack temperature, and input variables of the PEM fuel cell. Also, unlike conventional techniques, a neural network model does not need any linearization or assumptions in the model development. In conventional modeling approach, such assumptions and/or linearization may be necessary to reduce the overall complexity of the model. Also, since neural networks can map highly nonlinear relationships, without the necessity of determining process parameters, the model development process is relatively less tedious, which helps in reducing the time required for developing the model.

In the literature, some work on the PEM fuel cell modeling using a neural network approach is also reported. In [19], recurrent neural network models are proposed for the onboard fuel cell power supply. However, the models are proposed only for different fuel cell load current frequencies without any further study of the dynamic behavior of the PEM fuel cell. In [20] and [21], the PEM fuel cell is modeled using feedforward neural networks, but work does not provide any further analysis of the PEM fuel cell system using these models. In [22], the PEM fuel cell's stack temperature is modeled using artificial neural networks. However, the model is not trained for the PEM fuel cell's stack voltage values.

In this paper, the nonlinear autoregressive model of the 500-W PEM fuel cell with external inputs (NARMAX) is developed using recurrent neural networks. The data required to train the neural network model is generated by simulating the nonlinear state space model of the 500-W PEM fuel cell, developed in [1] by same authors. The model is trained for the PEM fuel cell's output voltage and stack temperature values and is extensively used to study the dynamic behavior of the PEM fuel cell. The paper is organized as follows: cross-correlation analysis is performed in Section II, Section III presents the neural network model development, Section IV analyzes the robustness of the trained neural network model toward noise, and Section V depicts the conclusion of this research study.

A. Operation of the PEM Fuel Cell

The PEM fuel cell consists of a polymer membrane placed between two electrodes that are coated with the platinum catalyst [2]. The hydrogen gas, extracted using reformer from the hydrocarbon fuel, is supplied at the anode. Air, a source of oxygen, is supplied at the cathode. At the anode, hydrogen gas, in the presence of platinum catalyst, is ionized into positively charged hydrogen ions and negatively charged electrons [2], [13].

The PEM permits only positively charged hydrogen ions to flow from the anode to the cathode. The negatively charged electrons from the anode have to reach the cathode via external circuit [13], [23]. This process leads to the generation of electric current. At the cathode, electrons and protons combine with oxygen from air to form water that flows out of the fuel cell [13].

The open-circuit output voltage of the PEM fuel cell can be given as [1], [2]

$$V_{O,\mathrm{FC}} = n_S E_0^{\mathrm{Cell}} + \frac{n_S RT}{2F} \ln\left[\frac{P_{\mathrm{H_2}} \left(P_{\mathrm{O_2}}\right)^{0.5}}{P_{\mathrm{H_2O}}}\right]. \quad (1)$$

However, at normal operating conditions, the actual output voltage of the PEM fuel cell is determined by irreversible voltage losses, present within the PEM fuel cell [2] . Three types of voltage losses exist: activation voltage loss, ohmic voltage loss, and concentration voltage loss.

The activation losses of a single PEM fuel cell stack can be modeled by the Tafel equation as [2], [13]

$$V_{\mathrm{loss}}^{\mathrm{Act}} = \frac{RT}{2F} \ln\left(\frac{I}{I_d}\right) = a_0 + T[a + b\ln(I)]. \quad (2)$$

The ohmic losses are due to the ohmic resistance of the PEM fuel cell and can be given as [2], [13]

$$V_{\mathrm{loss}}^{O} = I.R^0 = V_A^O + V_C^O + V_M^O. \quad (3)$$

The concentration losses exist due to the formation of concentration gradients of reactants at the surface of the electrodes [2]. For a single PEM fuel cell stack, concentration losses can be given as [2], [13]

$$V_{\mathrm{loss}}^{\mathrm{Conc}} = -\frac{RT}{eF} \ln\left(1 - \frac{I}{I_L}\right). \quad (4)$$

In the PEM fuel cell, since positive hydrogen ions reach the cathode through polymer membrane, and electrons reach the cathode via external circuit, two charged layers of opposite polarities are formed at the cathode [2], [13]. This charge double layer can store electrical charge and behaves like a capacitor. Hence, the voltage across this charge double layer cannot respond to change in the current immediately [2], [13]. This charge double layer plays an important role in determining the dynamic response of the PEM fuel cell. The voltage across this charge double layer can be given as [2], [13]

$$V_C = \left(I - C\frac{dV_C}{dt}\right)\left(R^{\mathrm{Act}} + R^{\mathrm{Conc}}\right). \quad (5)$$

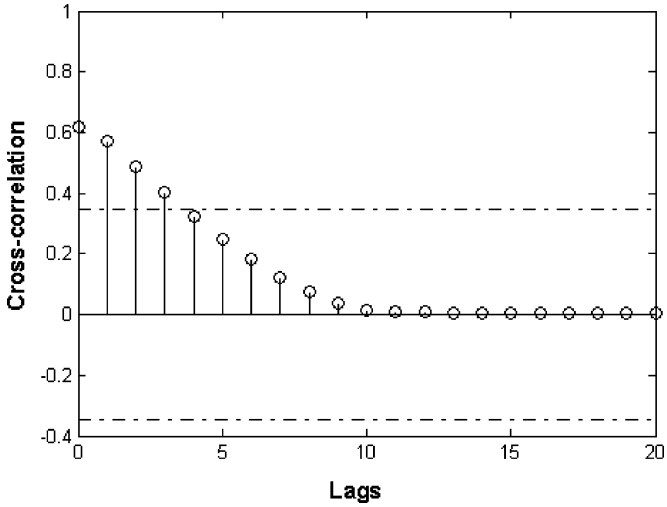

Fig. 2. Cross correlation between V_{fc} and $u_{\mathrm{P_A}}$.

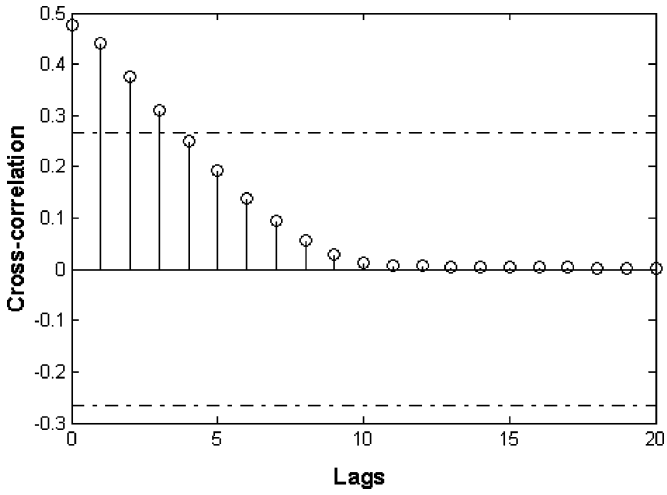

Fig. 3. Cross correlation between V_{fc} and $u_{\mathrm{P_C}}$.

The output voltage of the PEM fuel cell at normal operating conditions, in terms of voltage losses and voltage across charge double layer, can be given by (6) and (7) [1].

$$V_{\mathrm{fc}} = V_{O,\mathrm{FC}} - n_S\left(V_{\mathrm{loss}}^{\mathrm{Act}} + V_{\mathrm{loss}}^{O} + V_{\mathrm{loss}}^{\mathrm{Conc}}\right). \quad (6)$$

$$V_{\mathrm{fc}} = n_S E_0^{\mathrm{Cell}} + \left[\frac{n_S R}{2F} \ln\left(\frac{P_{\mathrm{H_2}} \left(P_{\mathrm{O_2}}\right)^{0.5}}{P_{\mathrm{H_2O}}}\right)\right] T - n_S\left[(a_0 + aT) - V_C - IR^O\right]. \quad (7)$$

The overall nonlinear state space model of the PEM fuel cell can be described by (8) and (9) [1]

$$\dot{x}(t) = A(\theta)x(t) + B(\theta)u(t) + G(\theta)w(t) \quad (8)$$

$$y(t) = C(\theta)x(t) + v(t). \quad (9)$$

where $x(t)$ represents the system states, $y(t)$ represents the system output, $u(t)$ is the control input, $w(t)$ is the disturbance input, which is the load current, and $v(t)$ is the measurement noise. The description of vectors $x(t), u(t), y(t)$ along with

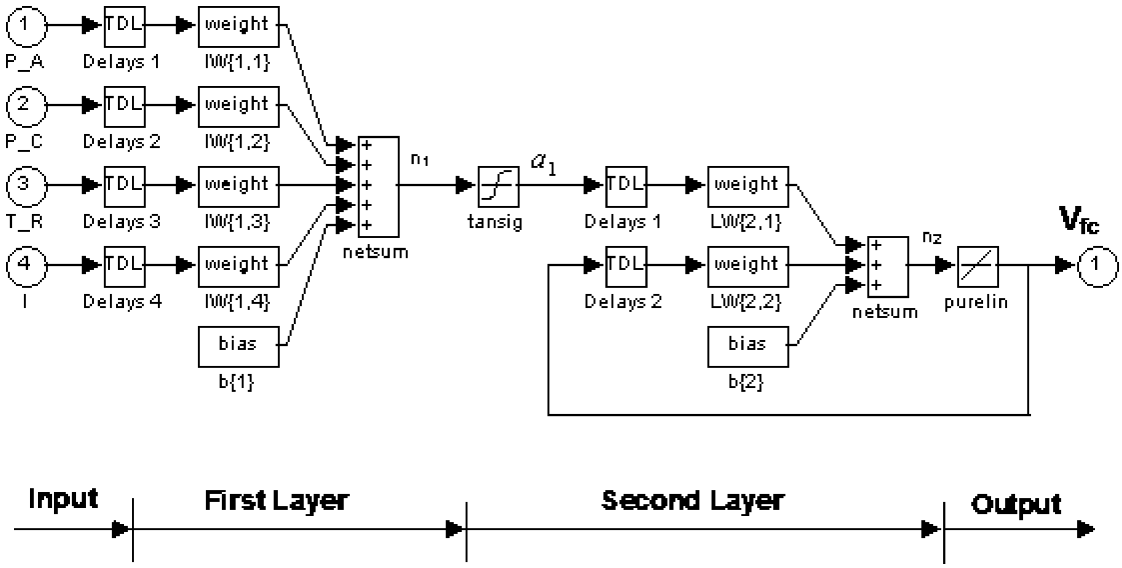

Fig. 5. Neural network model of the PEM fuel cell.

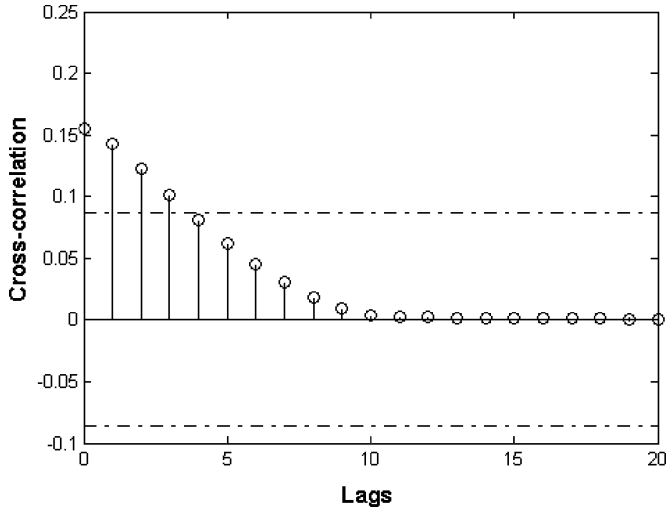

Fig. 4. Cross correlation between $V_{\rm fc}$ and $u_{\rm T_R}$.

matrices A, B, C, G, and state-dependent parameter vector θ are given in the Appendix.

II. Cross-Correlation Analysis

The cross-correlation analysis can be used to detect the interaction strength between two signals. The analysis can also be used to detect whether a time lag exists between the signals [24]. It has been proved in the literature that time-delay estimation between two continuous signals can be done by detecting peaks in the cross-correlation function [25]. In this paper, cross-correlation analysis is performed to determine the interaction strength between inputs variables and output voltage of the PEM fuel cell. Equation (10) shows the computation of the cross-correlation function [26]. Figs. 2, 3, and 4 show the results of cross correlation between the output voltage $V_{\rm fc}$ of the PEM fuel cell and input vectors $u_{\rm P_A}$, $u_{\rm P_C}$, and $u_{\rm T_R}$, respectively. The presence of peaks in these figures indicates a high degree of correlation between the data separated by the corresponding discrete time instant. The contributions of the output voltage $V_{\rm fc}$ on input variables $u_{\rm P_A}$, $u_{\rm P_C}$, and $u_{\rm T_R}$ decrease gradually with an increase in the value of lag. Thus, based on this study, it can be seen that the input vectors $u_{\rm P_A}$, $u_{\rm P_C}$, and $u_{\rm T_R}$ of the neural network model can be made sufficiently large to incorporate a large window of delayed measurements. However, very large number of lags will increase the size of the neural network's input layer, and the network will require more time to converge. Therefore, the sizing of the input vectors of the network is done based on the concept of parsimony [27], i.e., if the performance of the neural network model does not show any significant improvement with increase in the size of the input vector, then a fewer number of delays are used in the input vector [27].

$$\varphi_{\rm uy} = \lim_{T\to\infty} \frac{1}{2T} \int_{-T}^{T} u(t)y(t+\tau)dt. \tag{10}$$

Therefore, a different number of delays for input vectors $u_{\rm P_A}$, $u_{\rm P_C}$, and $u_{\rm T_R}$ are tried in the neural network model and, finally, input vectors $u_{\rm P_A}$, $u_{\rm P_C}$, and $u_{\rm T_R}$ are sized to incorporate six delays. It is observed that with the number of lags in the input vectors to be six, the neural network model can be trained satisfactorily. The lags are represented by "tapped delay line" block in the neural network model, as shown in Fig. 5.

III. Neural Network Model Development

A neural network is composed of simple elements (artificial neurons) operating in parallel. The network function is determined by the connections (weights) between the elements [8]. Also, by adjusting the values of the connections between elements, the neural network can be trained to approximate a given function. The structure of the proposed network to model the dynamic behavior of the PEM fuel cell is shown in Fig. 5. The dynamic behavior of the PEM fuel cell depends on change in the output current of the fuel cell. Hence, the output current is fed back to the model. The first layer is the input layer and the second layer is the output layer. A network with a different number of hidden neurons in the input layer is tried, and finally

the number of hidden neurons selected in the first layer is 35. A two-layer network with a hyperbolic tangent sigmoid function, as an activation function in the first layer, and a pure linear function, as an activation function in the second layer, can be used to model most nonlinearities [7], [8]. Hence, the hyperbolic tangent sigmoid function—"tansig (. .)" is chosen to be the activation function of the input layer. The relationship between a_1, the output of the first layer, and the input variables $u_{\mathrm{P_A}}, u_{\mathrm{P_C}}, u_{\mathrm{T_R}}, I$ is given by (11)

$$n_1 = IW\{1,1\}u_{\mathrm{P_A}} + IW\{1,2\}u_{\mathrm{P_C}} + IW\{1,3\}u_{\mathrm{T_R}} + IW\{1,4\}I + b\{1\} \tag{11}$$

where n_1 is the weighted sum of the input variables, which is fed to the hyperbolic tangent sigmoid transfer function.

$$a_1 = \tan\mathrm{sig}(n_1) = \left[\frac{2}{1+e^{-2n_1}} - 1\right]. \tag{12}$$

The output of the first layer a_1 is then fed to the second layer. A pure linear function is chosen to be the activation function of the second layer, which yields

$$n_2 = LW\{2,1\}a_1 + LW\{2,2\}V_{\mathrm{fc}} + b\{2\} \tag{13}$$

$$V_{\mathrm{fc}} = \mathrm{purelin}(n_2) \tag{14}$$

where n_2 is the weighted sum fed to the linear function in the second layer of the network. The output V_{fc} is fed back at the input of the second layer to create the recurrent network that helps in quicker convergence. The linear activation function is chosen in the output layer, as it can distribute the target values and can handle potential deficiencies associated with the requirements to extrapolate beyond the range of the training dataset. It also restricts potential impact and distortions associated with upper and lower limit saturation effects [29].

A. Training of the Neural Network Model

The data used for training the neural network model is obtained by simulating the nonlinear state space model of the PEM fuel cell developed in [1]. Five input–output data sets with different values of $u_{\mathrm{P_A}}, u_{\mathrm{P_C}}, u_{\mathrm{T_R}}, I$ are used as the training data sets. Each data set consists of 120 data samples of each input variable. The values utilized for the input variables are $u_{\mathrm{P_A}}$ is varied from 5 to 30 atm, $u_{\mathrm{P_C}}$ is varied from 5 to 40 atm, $u_{\mathrm{T_R}}$ is varied from 298 to 318 K, and I is varied from 1 to 25 A. Overall, 4800 data points are used to train the model for the PEM fuel cell's output voltage and stack temperature values. The Levenberg–Marquardt backpropagation algorithm is used for training, which is performed using the neural network toolbox of MATLAB/Simulink [8]. The performance of the trained network for the output voltage values is shown in Fig. 6. The convergence criterion for training the model is set to 10^{-5} V. After training the model for 400 epochs, the mean-squared voltage error observed is $1.866.10^{-3}$ V.

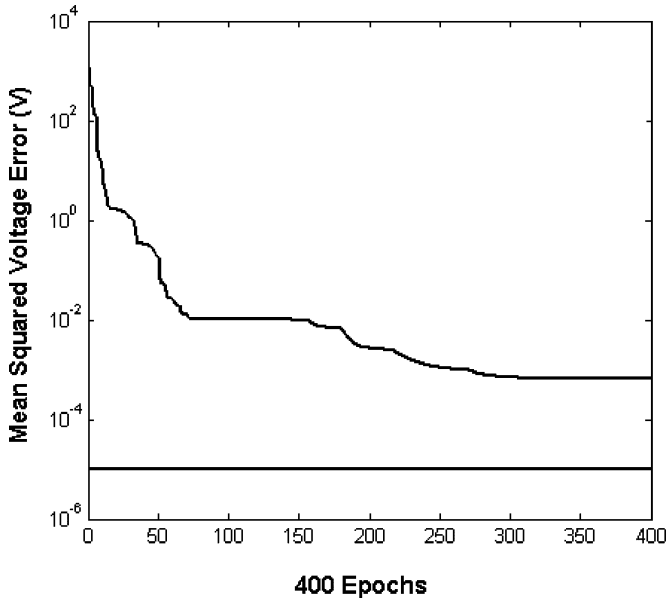

Fig. 6. Training of the neural network model for output voltage values.

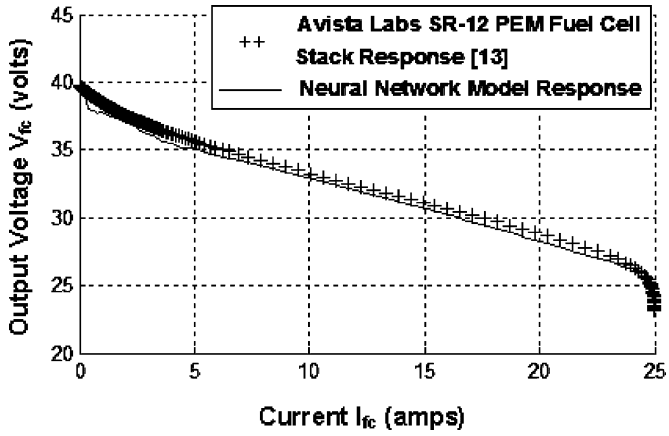

Fig. 7. Validation of the neural network model of the PEM fuel cell.

B. Simulation Results

The trained neural network model is simulated for the following values of input variables: $u_{\mathrm{P_A}} = 1.8$ atm, $u_{\mathrm{P_C}} = 1$ atm, $u_{\mathrm{T_R}} = 308$ K. The simulation results are validated with the experimental results of the Avista Labs SR-12 PEM fuel cell stack presented in [13]. Fig. 7 shows the comparison of the *V–I* characteristics of the neural network model with the *V–I* characteristics of the Avista Labs SR-12 PEM fuel cell stack obtained experimentally. The validation results show a close match. Please note that, in [13], experimental results of the Avista Labs SR-12 (500 W) PEM fuel cell stack are given, and the *V–I* characteristics obtained by simulating the neural network model developed in this paper are compared with the experimental *V–I* characteristics presented in [13].

As training of the neural network model is performed with the data generated by the state space model, and not directly with the experimental PEM fuel cell data, it is important to check the degree of compliance of the state space model with the actual experimental results. Hence, the simulation results of the state

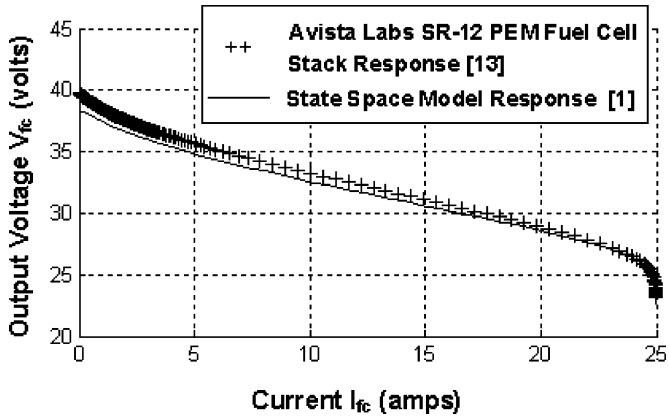

Fig. 8. Validation of the state space model of the PEM fuel cell.

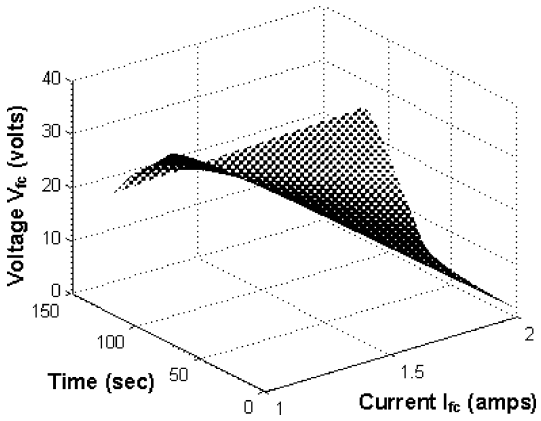

Fig. 9. Polarization characteristics of the neural network model.

space model, developed in [1], are also validated with the experimental data of the Avista Labs SR-12 PEM fuel cell stack given in [13]. The comparison is shown in Fig. 8.

Fig. 9 shows the polarization characteristics or the *V–I* characteristics of the PEM fuel cell model with respect to time in a 3-D plane, obtained by simulating the model at $u_{\mathrm{P_A}} = 1.5$ atm, $u_{\mathrm{P_C}} = 1$ atm, and $u_{\mathrm{T_R}} = 303$ K.

The output voltage response of the neural network model is shown in Fig. 10 . To obtain this output voltage response, the current is varied from 1 to 25 A, in steps of 0.4 A, every 40 s over a total simulation period of 2720 s. It is seen that the output voltage decreases from about 41 to 24 V as the current is increased. The response is compared with the output voltage response of the state space model.

The power versus current characteristics obtained by simulating the neural network model is shown in Fig. 11. It can be seen that the maximum output power is obtained close to the fuel cell rated current (25 A) but not exactly at the rated current. The PEM fuel cell goes in the concentration region near rated current value. In this region, the output voltage of the PEM fuel cell drops sharply due to an increase in the current. This leads to the decrease in the output power of the PEM fuel cell [2], [13].

The neural network model is also trained for the stack temperature values, and the performance of the trained network is shown in Fig. 12. The convergence criterion for the training is

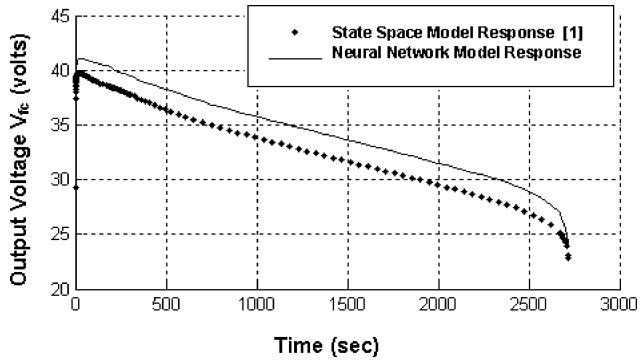

Fig. 10. Output voltage response of the neural network model.

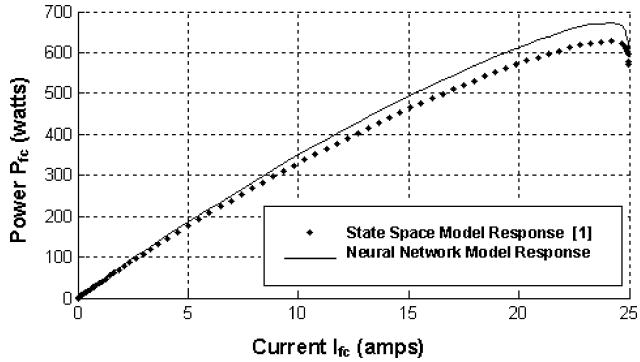

Fig. 11. Power versus current characteristics of the neural network model.

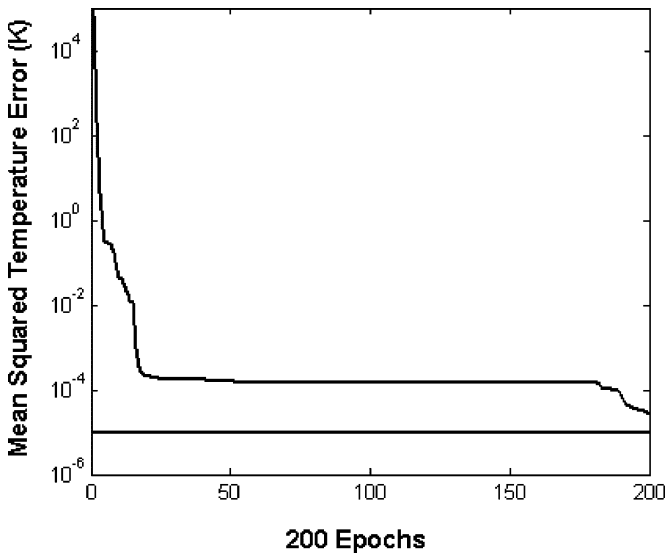

Fig. 12. Training of the neural network model for stack temperature values.

set to be 10^{-5} K and after training the model for 200 epochs, the mean-squared temperature error observed is $2.779.10^{-5}$ K.

To obtain the temperature response, the neural network model is simulated for the following values of input variables: $u_{\mathrm{P_A}} = 2.5$ atm, $u_{\mathrm{P_C}} = 1$ atm, and $u_{\mathrm{T_R}} = 308$ K. Fig. 13 shows the temperature response of the model. The response is compared with the temperature response of the state space model in [1]. The comparison shows a close match. It can be seen that, as

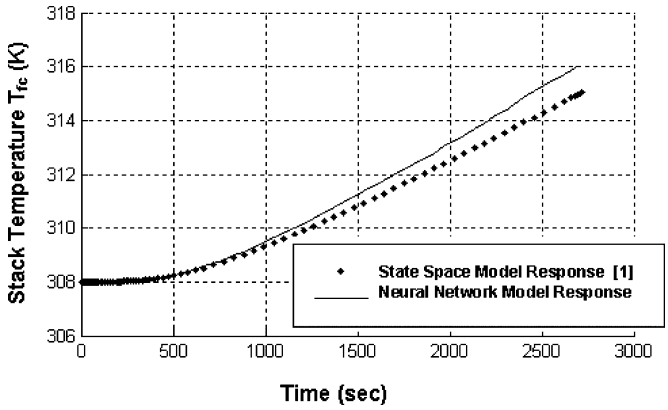

Fig. 13. Temperature response of the neural network model.

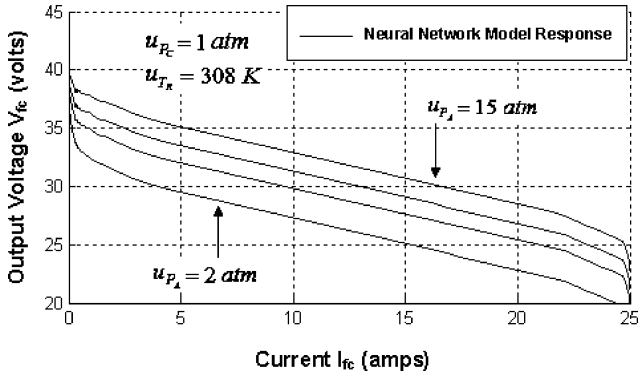

Fig. 14. *V–I* Characteristics of the PEM fuel cell model for increasing $u_{\mathrm{P_A}}$.

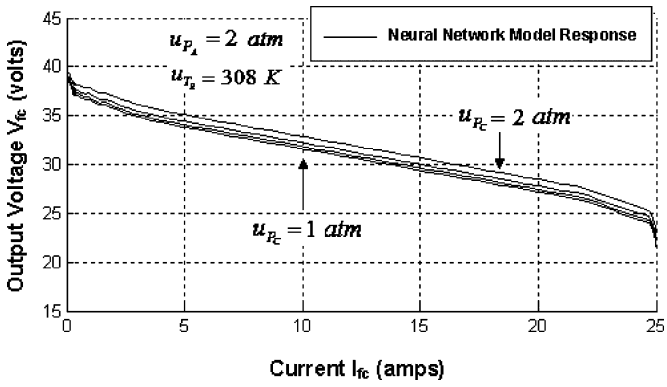

Fig. 15. *V–I* Characteristics of the PEM fuel cell model for increasing $u_{\mathrm{P_C}}$.

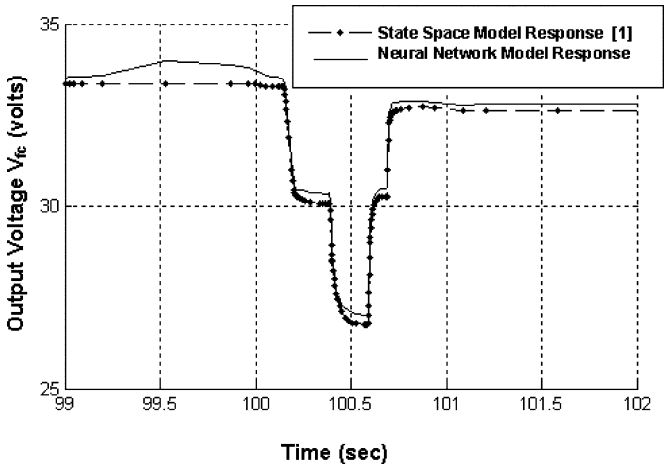

Fig. 16. Transient response of the model over a short-time period.

electrochemical reaction proceeds within the PEM fuel cell, the stack temperature rises from 308 to 316 K.

C. Polarization Curves of the PEM Fuel Cell Model for Different Values of Input Variables

A neural network model is subjected to different values of input variables in order to study their effect on the *V–I* characteristics, output voltage, and voltage losses of the PEM fuel cell. Fig. 14 shows the *V–I* characteristics obtained by simulating the neural network model for different values of $u_{\mathrm{P_A}}$. The model is simulated for: $u_{\mathrm{P_A}} = 2, 5, 8,$ and 15 atm. The other two input variables $u_{\mathrm{P_C}}$ and $u_{\mathrm{T_R}}$ are kept constant at 1 atm and 308 K, respectively.

Fig. 15 shows the *V– I* characteristics obtained by simulating the neural network model for increasing values of $u_{\mathrm{P_C}}$. The model is simulated for: $u_{\mathrm{P_C}} = 1, 1.5, 1.8,$ and 2 atm. The other two input variables $u_{\mathrm{P_A}}$ and $u_{\mathrm{T_R}}$ are kept constant at 2 atm and 308 K, respectively.

From Figs. 14 and 15, it can be seen that as $u_{\mathrm{P_A}}$ and $u_{\mathrm{P_C}}$ are increased, the output voltage of the PEM fuel cell increases, which reduces voltage losses in the PEM fuel cell. For higher values of $u_{\mathrm{P_A}}$ and $u_{\mathrm{P_C}}$, voltage losses are smaller. Hence, it is possible to reduce voltage losses in the PEM fuel cell by operating the PEM fuel cell at higher values of $u_{\mathrm{P_A}}$ and $u_{\mathrm{P_C}}$.

It must be noted that neural network model of PEM fuel cell cannot be used to compute the value of any individual voltage losses within PEM fuel cell. The model can only determine overall change in the value of voltage losses as a function of input variables.

D. Transient Response of the PEM Fuel Cell Model

A trained neural network model of the PEM fuel cell can be used to study the transient response of the model over a short- and longtime periods. Fig. 16 shows the transient response of the model over a short-time period. The model is simulated for $u_{\mathrm{P_A}} = 2.5$ atm, $u_{\mathrm{P_C}} = 1$ atm, $u_{\mathrm{T_R}} = 308$ K. The input variable $I$of the model is varied in steps over a small time period between 99 to 102 s to observe the transient behavior. It can be seen that as the load is increased, the output voltage drops and vice versa. However, the output voltage does not reach new value immediately. As the load is increased, the voltage drops to a certain value immediately, but from there it reaches to its new value in an exponential manner. This is due to the capacitance of the charge double layer formed on the surface of the cathode. Higher the value of the capacitance, longer it takes for the voltage to reach its new value [2], [13]. Hence, the transient response of the PEM fuel cell over a short-time period depends on the capacitance of the charge double layer.

The transient response of the neural network model over a long-time period is shown in Fig. 17. It is observed that as the load current is changed, the output voltage changes to a certain value, and from there it reaches to its final value in few hundred

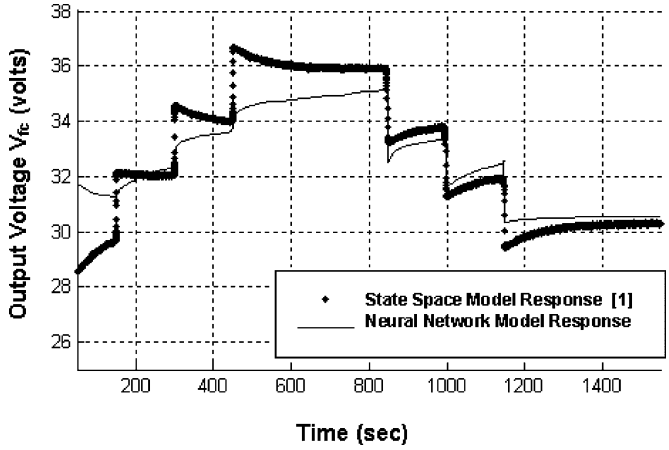

Fig. 17. Transient response of the model over a longtime period.

TABLE I
MEAN-SQUARED VOLTAGE ERRORS FOR DIFFERENT SNRS

Signal-to-Noise Ratio (SNR)	Mean Squared Voltage Error
No noise	$1.866.10^{-3}$
1000:1	$2.779.10^{-3}$
800:1	$8.625.10^{-3}$
500:1	$3.39.10^{-2}$
200:1	$7.971.10^{-2}$
100:1	$9.142.10^{-2}$
50:1	$9.912.10^{-2}$
10:1	$1.032.10^{-1}$

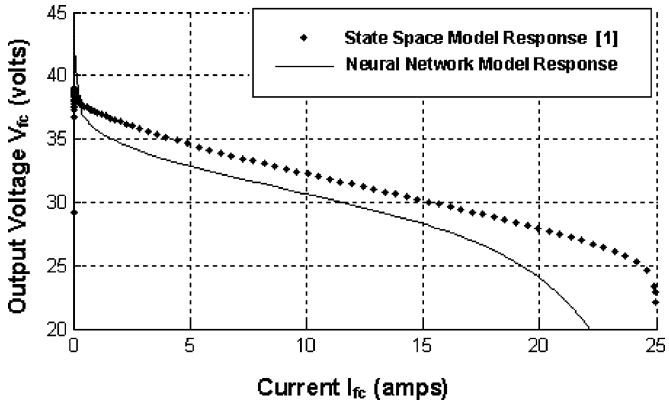

Fig. 18. Performance of the neural network model for SNR 200:1.

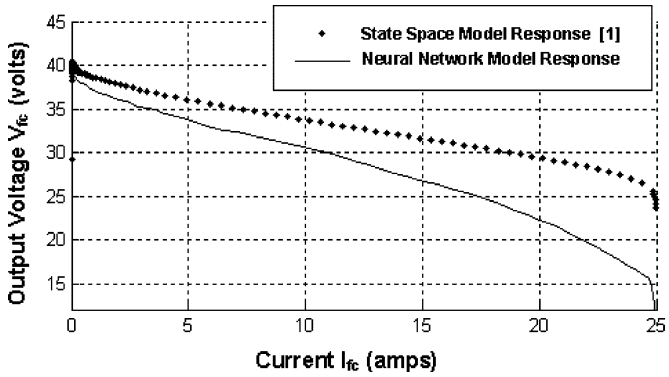

Fig. 19. Performance of the neural network model for SNR 50:1.

seconds. This type of response is observed due to the higher thermodynamic time constant, as well as due to air and hydrogen flow delays inside the PEM fuel cell. These delays can vary from few seconds to few minutes in the PEM fuel cell [5], [13].

It can be seen from Fig. 13 that the change in the temperature of the PEM fuel cell stack takes certain time as electrochemical reaction proceeds in the PEM fuel cell. i.e., the stack temperature cannot change immediately. This makes thermodynamic time constant of the PEM fuel cell higher. Similarly, hydrogen and airflows to the anode and cathode cannot immediately follow the changes in the load [13]. Hence, it can be concluded that the transient response of the PEM fuel cell over a long-time period depends on the thermodynamic time constant of the PEM fuel cell and flow delays within the PEM fuel cell [5], [13].

IV. ROBUSTNESS TOWARD NOISE

To investigate the effect of measurement noise on the performance of the neural network model, noise-corrupted measurements are generated by adding zero mean independent white Gaussian noise-to-noise free signals. These noise-corrupted signals are then applied to the neural network model of the PEM fuel cell. The equations used to generate noise-corrupted signals are given in [28].

The results of application of noise-corrupted data, with different SNR levels, to the neural network model are tabulated in Table I. For sake of comparison, the mean-squared voltage error for noise-free case is also listed. It can be seen that with low-SNR levels (large amount of noise), the performance of the model deteriorate significantly with corresponding increase in the mean-squared voltage error. The performance of the neural network model for SNRs 200:1 and 50:1 is shown in Figs. 18 and 19, respectively.

V. CONCLUSION

In this paper, nonlinear autoregressive model of the 500-W PEM fuel cell is developed using recurrent neural networks. It is shown that the nonlinear dynamics of the PEM fuel cell can be effectively modeled using two-layer recurrent neural network. The data required to train the neural network model is generated by simulating the nonlinear state space model of the PEM fuel cell developed in [1]. The neural network model is trained for the PEM fuel cell's output voltage and stack temperature values. To prove the effectiveness of the model, it is validated with the experimental results of the Avista Labs SR-12 (500 W) PEM fuel cell stack presented in [13]. The model is then used to analyze the dynamic behavior of the PEM fuel cell. Polarization curves are obtained by subjecting the model to different values of input variables, and it is found that voltage losses in the PEM fuel cell can be reduced by operating the PEM fuel cell at higher values of input variables. The transient behavior of the PEM fuel cell over short and long-time periods is studied, and it is found that the transient response of the PEM fuel cell over a short-time period depends on the capacitance of the charge double layer formed at the surface of the cathode. The transient response of

the PEM fuel cell over a long-time period depends on the thermodynamic time constant and flow delays within the PEM fuel cell. Finally, the robustness of the trained neural network model toward noise is analyzed. It is shown that low-SNR levels increase the mean-squared voltage error, which results in deterioration of the performance of the neural network model.

APPENDIX

$$x = [(m_{\mathrm{O}_2})_{\mathrm{net}} \quad (m_{\mathrm{H}_2})_{\mathrm{net}} \quad (m_{\mathrm{H}_2\mathrm{O}})_{\mathrm{net}} \quad T \quad P_{\mathrm{H}_2} \quad P_{\mathrm{O}_2} \quad P_{\mathrm{H}_2\mathrm{O}} \quad Q_C \quad Q_E \quad Q_L \quad V_C]^T$$

$$u = [u_{\mathrm{P_A}} \quad u_{\mathrm{P_C}} \quad u_{\mathrm{T_R}}]^T \qquad w = [I]$$

and A and B shown at the bottom of this page,

$$y = \theta_7(x_4, x_5, x_6, x_7)$$

$$\theta = [\theta_1(x_4) \quad \theta_2(x_4) \quad \theta_3(x_4) \quad \theta_4(x_4) \quad \theta_5(x_7) \quad \theta_6(x_4, x_5, x_6, x_7) \quad \theta_7(x_4, x_5, x_6, x_7) \quad \theta_8(x_4, x_5, x_6, x_7)]^T$$

$$A_{4\times 4} = \left[\frac{-h_S n_S A_S}{M_{\mathrm{fc}} C_{\mathrm{fc}}}\right] \qquad A_{11\times 11} = \left[\frac{-1}{C(R^{\mathrm{Act}} + R^{\mathrm{Conc}})}\right]$$

$$G = \left[\left(\frac{1}{4\lambda_C F}\right) \quad \left(\frac{1}{2\lambda_A F}\right) \quad \left(\frac{1}{2\lambda_C F}\right) \quad -\theta_8(x_4, x_5, x_6, x_7) \quad -\theta_2(x_4) \quad -\theta_4(x_4) \quad 2\theta_4(x_4) \quad \theta_6(x_4, x_5, x_6, x_7) \quad \theta_7(x_4, x_5, x_6, x_7) \quad 0 \quad \frac{1}{C}\right]^T.$$

ACKNOWLEDGMENT

The authors would like to thank Prof. Nehrir for their use of the experimental test data for the model validation in this paper.

REFERENCES

[1] S. Puranik and A. Keyhani., Sep. 2007, Dynamic modeling of proton exchange membrane fuel cell. Mechatronic-Green Energy Syst. Lab., Ohio State Univ.. Columbus, Tech. Rep. TR040. [Online]. Available: http://www.ece.osu.edu/ems/files/TechnicalReports.html, [Online]. Available:

[2] J. Larminie and A. Dicks, *Fuel Cell Systems Explained*, 1st ed. New York: Wiley , 2000, pp. 29–52.

[3] M. W. Ellis, M. R. Von Spakovsky, and D. J. Nelson, "Fuel cell systems: Efficient, flexible energy conversion for the 21st century," *Proc. IEEE*, vol. 89 , no. 12, pp. 1808–1818, Dec. 2001.

[4] "Fuel Cell Works Industry News and Information Leader.," in 2007 [Online]. Available: http://fuelcellworks.com/, [Online]. Available:

[5] J. T. Pukrushpan , A. G. Stefanopoulou, and H. Peng, "Control of fuel cell breathing," *IEEE Control Syst. Mag.*, vol. 24, no. 2, pp. 30–46, Apr. 2004 .

[6] M. Tanrioven and M. S. Alam, "Modeling, control, and power quality evaluation of a PEM fuel cell-based power supply system for residential use," *IEEE Trans. Ind. Appl.*, vol. 42, no. 6 , pp. 1582–1589, Nov./Dec. 2006.

[7] G. Calderon, J.-P. Draye, D. Pavisic, R. Teran, and G. Libert, "Nonlinear dynamic system identification with dynamic recurrent neural networks," in *Proc. Int. Workshop Neural Netw. Identification, Control, Robot., Signal/Image Process.*, Aug. 21--23, 1996, pp. 49–54.

[8] "Neural Network Toolbox (Version 5.0.2), MATLAB 7.4.0.287 (R2007a).," in 2007 [Online]. Available: http://www.mathworks.com/access/helpdesk/help/toolbox/nnet/, [Online]. Available:

[9] J. C. Amphlett , R. M. Baumert, R. F. Mann, B. A. Peppley , P. R. Roberge, and T. J. Harris, " Performance modeling of the Ballard mark IV solid polymer electrolyte fuel cell, I. Mechanistic model development ," *J. Electrochem. Soc.*, vol. 142, no. 1, pp. 1–8, Jan. 1995.

[10] J. C. Amphlett , R. M. Baumert, R. F. Mann, B. A. Peppley , P. R. Roberge, and T. J. Harris, "Performance modeling of the Ballard mark IV solid polymer electrolyte fuel cell II. Empirical model development," *J. Electrochem. Soc.*, vol. 142, no. 1, pp. 9 –15, Jan. 1995.

[11] T. E. Springer , T. A. Zawodzinski, and S. Gottesfeld, "Polymer electrolyte fuel cell model," *J. Electrochem. Soc.*, vol. 138, no. 8 , pp. 2334–2342, Aug. 1991 .

[12] S. Pasricha and S. R. Shaw, "A dynamic PEM fuel cell model," *IEEE Trans. Energy Convers.* , vol. 21, no. 2, pp. 484–490, Jun. 2006.

[13] C. Wang, M. H. Nehrir, and S. R. Shaw, "Dynamic models and model validation for PEM fuel cells using electrical circuits," *IEEE Trans. Energy Convers.*, vol. 20, no. 2, pp. 442–451, Jun. 2005.

[14] L.Y. Chiu and B. M. Diong, "An improved small-signal model of the dynamic behavior of PEM fuel cells," in *Proc. IEEE 38th IAS Annu. Meet.*, Oct. 2003, vol. 2, pp. 709–715.

[15] W. Friede, S. Rael, and B. Davat, "Mathematical model and characterization of the transient behavior of a PEM fuel cell," *IEEE Trans. Power Electron.*, vol. 19, no. 5, pp. 1234–1241, Sep. 2004.

[16] D. Yu and S. Yuvarajan, "A novel circuit model for PEM fuel cells," in *Proc. 19th Annu. IEEE APECE* , 2004, vol. 1, pp. 362–366 .

[17] M. Uzunoglu and M. S. Alam, "Dynamic modeling, design, and simulation of a combined PEM fuel cell and ultracapacitor system for stand-alone residential applications," *IEEE Trans. Energy Convers.*, vol. 21, no. 3, pp. 767–775, Sep. 2006.

[18] C. Wang, M. H. Nehrir, and H. Gao, "Control of PEM fuel cell distributed generation systems," *IEEE Trans. Energy Convers.*, vol. 21, no. 2, pp. 586–595, Jun. 2006.

$$A = \begin{bmatrix} \frac{-1}{\lambda_C} & 0 & 0 & 0 & 0 & 0 & 0_{1\times 4} & 0 \\ 0 & \frac{-1}{\lambda_A} & 0 & 0 & 0 & 0 & 0_{1\times 4} & 0 \\ 0 & 0 & \frac{-1}{\lambda_C} & 0 & 0 & 0 & 0_{1\times 4} & 0 \\ 0 & 0 & 0 & A_{4\times 4} & 0 & 0 & 0_{1\times 4} & 0 \\ 0 & 0 & 0 & 0 & -2\theta_1(x_4) & 0 & 0_{1\times 4} & 0 \\ 0 & 0 & 0 & 0 & 0 & -2\theta_3(x_4) & 0_{1\times 4} & 0 \\ 0 & 0 & 0 & 2\theta_5(x_7) & 0 & 0 & 0_{1\times 4} & 0 \\ 0_{2\times 1} & 0_{2\times 1} & 0_{2\times 1} & 0_{2\times 1} & 0_{2\times 1} & 0_{2\times 1} & 0_{2\times 4} & 0_{2\times 1} \\ 0 & 0 & 0 & (h_S n_S A_S) & 0 & 0 & 0 & 0 \\ 0 & 0 & 0 & 0 & 0 & 0 & 0_{1\times 4} & A_{11\times 11} \end{bmatrix}$$

$$B = \begin{bmatrix} 0_{31} & 0_{3\times 1} & 0_{3\times 1} \\ 0 & 0 & \left(\frac{h_S n_S A_S}{M_{\mathrm{fc}} C_{\mathrm{fc}}}\right) \\ 2\theta_1(x_4) & 0 & 0 \\ 0 & 2\theta_3(x_4) & 0 \\ 0_{3\times 1} & 0_{3\times 1} & 0_{3\times 1} \\ 0 & 0 & (-h_S n_S A_S) \\ 0 & 0 & 0 \end{bmatrix}$$

[19] S. Jemei, D. Hissel, M. C. Pera, and J. M. Kauffmann, "Dynamical recurrent neural network towards modeling of on-board fuel cell power supply," in *Proc. IEEE Int. Symp. Ind. Electron.*, May 2004, vol. 1, pp. 471–476.
[20] S. Jemei, D. Hissel, M. C. Pera, and J. M. Kauffmann, "Black box modeling of proton exchange membrane fuel cell generators ," in *Proc. 28th Annu. Conf. Ind. Electron. Soc. (IECON)*, Nov. 2002 , vol. 2, pp. 1474–1478.
[21] M. Hatti, M. Tioursi, and W. Nouibat, "Static modelling by neural networks of a PEM fuel cell," in *Proc. IEEE 32nd Annu. Conf. Ind. Electron. (IECON)*, Nov. 2006, pp. 2121–2126.
[22] S. Tao, Y. Si-jia, C. Guang-yi, and Z. Xin-jian, "Modeling and control PEMFC using fuzzy neural networks," *J. Zhejiang Univ. Sci.*, vol. 6, pp. 1084–1089 , 2005.
[23] "U. S. Department of Energy website," in Energy Efficiency and Efficient Energy. 2008 [Online]. Available: http://www.eere.energy.gov/, [Online]. Available:
[24] M. El-Gohary, J. Mcnames, T. Ellis, and B. Goldstein, "Time delay and causality in biological systems using whitened cross-correlation analysis," in *Proc. 28th IEEE EMBS Conf.*, New York City, Aug. 2006, pp. 6169–6172 .
[25] C. H. Knapp and G. C. Carter, "The generalized correlation method for estimation of time delay," *IEEE Trans. Acoust., Speech Signal Process.*, vol. 24, no. 4, pp. 320 –327, Aug. 1976.
[26] L. C. Benn, B. Burton, and R. G. Harley, "Online converter fed induction motor impulse response identification and parameter extraction using pseudorandom modified PWM," in *Proc. 4th IEEE Int. Symp. Diagn. Electr. Mach., Power Electron. Drives*, Aug. 2003, pp. 70–75.
[27] S. Pillutla and A. Keyhani, "Development and implementation of neural network observers to estimate the state vector of a synchronous generator from on-line operating data," *IEEE Trans. Energy Convers.* , vol. 14, no. 4, pp. 1081–1087, Dec. 1999.
[28] S. Pillutla, A. Keyhani, and I. Kamwa, "Neural network observers for on-line tracking of synchronous generator parameters," *IEEE Trans. Energy Convers.*, vol. 14, no. 1, pp. 23–30, Mar. 1999.
[29] R. J. Abrahart and C. W. Dawson, "Neural network hydrological modelling: Linear Output Activation Functions?," *Amer. Geophys. Union*, Abstract #H54B-03, Fall Meeting, 2005, Fall Meeting.

Sachin V. Puranik (S'02–M'10) was born in Thane, India, on May 21, 1979. He received the B.E. degree in instrumentation and control engineering from the University of Mumbai, Maharashtra, India, in 2000, the M.S. degree in electrical engineering from Mississippi State University, Starkville, in 2004, and the Ph.D. degree from The Ohio State University, Columbus, in 2009.

He is now with Hubbell Power Systems, Leeds, AL. His current research interests include control of smart grid power systems, development of intelligent devices (IEDs) for smart grid power systems, modeling and control of distributed generation and green energy systems.

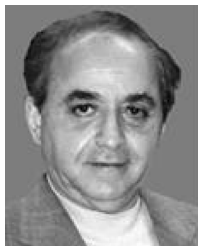

Ali Keyhani (S'72–M'76–SM'89–F'98) received the B.E., M.S.E.E., and Ph.D. degrees from Purdue University, West Lafayette, IN, in 1967, 1973, and 1976, respectively.

He is currently a Professor of electrical engineering at The Ohio State University (OSU), Columbus. He is also the Director of the OSU Electromechanical and Mechatronic Systems Laboratory. From 1967 to 1972, he was with Hewlett-Packard Company and TRW Control, Palo Alto, CA. His current research interests include control of distributed energy systems, power electronics, multilevel converters, power systems control, alternative energy systems, fuel cells, photovoltaic cells, microturbines, distributed generation systems, and parameter estimation and control of electromechanical systems.

Prof. Keyhani was the Past Chairman of the Electric Machinery Committee of IEEE Power Engineering Society and the Past Editor of the IEEE TRANSACTIONS ON ENERGY CONVERSION. He was the recipient of The Ohio State University College of Engineering Research Award for 1989, 1999, and 2003.

Farshad Khorrami (S'85–M'88–SM'96) received the B.S. degrees in mathematics and electrical engineering, the M.S. degree in mathematics, and the Ph.D. degree in electrical engineering, all from The Ohio State University, Columbus, in 1982, 1984, 1984, and 1988, respectively.

He is currently a Professor of electrical and computer engineering at the Polytechnic University, Brooklyn, NY, Where he has developed and directed Control/Robotics Research Laboratory. He is the author or coauthor of more than 180 refereed journal and conference papers and is the author of *Modeling and Adaptive nonlinear Control of Electric Motors* (Springer-Verlag, 2003). He is the holder of 12 U.S. patents on novel smart micropositioners and actuators, control systems, and wireless sensors and actuators. His research interest include adaptive and nonlinear control, large scale systems and decentralized control, unmanned autonomous vehicles, smart structures, robotics and high-speed positioning applications, and microprocessor-based control and instrumentation.

Prof. Khorrami has served on the program committees of several conferences and has been a Member of Conference Editorial Board of the IEEE Control Systems Society.